Λ and Σ^0 Pair Production in Two-Photon Collisions at LEP

The L3 Collaboration

Abstract

Strange baryon pair production in two-photon collisions is studied with the L3 detector at LEP. The analysis is based on data collected at e^+e^- centre-of-mass energies from 91 GeV to 208 GeV, corresponding to an integrated luminosity of 844 pb^{-1}. The processes $\gamma\gamma \to \Lambda\overline{\Lambda}$ and $\gamma\gamma \to \Sigma^0\overline{\Sigma}^0$ are identified. Their cross sections as a function of the $\gamma\gamma$ centre-of-mass energy are measured and results are compared to predictions of the quark-diquark model.

1 Introduction

Electron-positron colliders are a suitable place for the study of two-photon interactions, via the process $e^+e^- \rightarrow e^+e^-\gamma^*\gamma^* \rightarrow e^+e^-X$, where γ^* denotes a virtual photon. The outgoing electron and positron carry almost the full beam energy and are usually undetected, due to their small transverse momenta. The final state X has, therefore, a low mass relative to the e^+e^- centre-of-mass energy, $\sqrt{s}$. The small photon virtuality allows the extraction of the cross section $\sigma(\gamma\gamma \rightarrow X)$ in real photon collisions, once the photon flux is calculated by QED [1].

The process $\gamma\gamma \rightarrow$ *baryon antibaryon* is sensitive to the quark structure of the baryon. Calculations of the cross section for this process were performed using the hard scattering approach [2]. Due to the failure of a three-quark calculation [3] to correctly predict the $\gamma\gamma \rightarrow p\overline{p}$ cross section in the GeV region [4], an alternative quark-diquark model was proposed [5]. This model includes non-perturbative effects through the use of diquarks, a qq bound state within the baryon [6].

In this letter we present the first measurements at LEP of the cross sections $\sigma(\gamma\gamma \rightarrow \Lambda\overline{\Lambda})$ and $\sigma(\gamma\gamma \rightarrow \Sigma^0\overline{\Sigma}^0)$. We analysed a total integrated luminosity of 844 pb^{-1} collected with the L3 detector [7]. Out of this sample, 157 pb^{-1} were collected around the Z peak and 687 pb^{-1} at centre-of-mass energies from 161 GeV to 208 GeV. The analysis is based on the central tracking system and the high resolution BGO electromagnetic calorimeter. The events are selected by the track triggers [8].

Monte Carlo events are generated [9] for each beam energy and for each process within the formalism of Reference 1. An uniform spectrum as a function of the two-photon mass, $W_{\gamma\gamma}$, from threshold to 5 GeV is used. The two-body final states $\Lambda\overline{\Lambda}$ and $\Sigma^0\overline{\Sigma}^0$ are generated isotropically in the centre-of-mass of the $\gamma\gamma$ system. The events are then passed through the full L3 detector simulation using the GEANT [10] and GEISHA [11] programs and are reconstructed following the same procedure as for the data. Time dependent detector inefficiencies, as monitored during the data taking period, are taken into account.

The CLEO, TPC/2γ and VENUS collaborations [12–14] searched for the reaction $e^+e^- \rightarrow e^+e^-\Lambda\overline{\Lambda}$ at $\sqrt{s} = 10.6$ GeV, 14.5 GeV and 58 GeV, respectively. Only CLEO and TPC/2γ observe a signal. No results for the $e^+e^- \rightarrow e^+e^-\Sigma^0\overline{\Sigma}^0$ cross section were reported so far. Our results are compared to these experiments and to theoretical predictions of the quark-diquark model.

2 Event selection

In order to study the $\Lambda\overline{\Lambda}$ and $\Sigma^0\overline{\Sigma}^0$ final states, the $\Sigma^0 \rightarrow \Lambda\gamma$, $\overline{\Sigma}^0 \rightarrow \overline{\Lambda}\gamma$, $\Lambda \rightarrow p\pi^-$ and $\overline{\Lambda} \rightarrow \overline{p}\pi^+$ decays are considered. The preselection of events is based on charged tracks and proceeds as follows:

- There must be four charged tracks in the tracking chamber with a net charge of zero. These tracks must be reconstructed from at least 12 hits out of a maximum of 62.

- There must be two secondary vertices at a distance from the primary interaction vertex greater than 3 mm in the transverse plane.

- The angle in the transverse plane between the flight direction of each Λ candidate and the total momentum vector of the two outgoing tracks must be less than 0.15 rad.

- Events with a secondary vertex due to a photon conversion are rejected. A conversion is identified if by assigning the electron mass to the two tracks, their effective mass is below 0.05 GeV.

2.1 Λ identification

The two secondary vertices are assigned to the Λ and $\overline{\Lambda}$ decays. At each vertex, the p or the $\overline{p}$ are identified as the highest momentum tracks. Monte Carlo studies show that this is the correct configuration in more than 99% of the cases. To suppress the dominant $e^+e^- \to e^+e^- K_s^0 K_s^0 \to e^+e^- \pi^+\pi^-\pi^+\pi^-$ background, the following criteria are applied:

- The dE/dx measurement must be consistent with the Λ or $\overline{\Lambda}$ hypotheses. A confidence level CL > 0.001 is required for both proton, antiproton and pions candidates. This cut rejects 85% of the $K_s^0 K_s^0$ background.

- The particle assignment is considered to be correct if either,

  a) there is at least one of the tracks associated to a proton or to an antiproton with more than 30 hits and a dE/dx confidence level ratio $CL(p)/CL(\pi) > 10$, or

  b) the ratio between the electromagnetic transverse energy, E_T, and the transverse momentum, p_T, of the antiproton candidate is greater than 0.7. This cut eliminates 70% of the pions and keeps 77% of the antiproton signal, as shown in Figure 1.

  The dE/dx identification has a high discriminating power for particles with momentum below 700 MeV, whereas the E_T/p_T cut becomes more efficient for higher momentum antiprotons. These criteria suppress 83% of the remaining $K_s^0 K_s^0$ background.

- If two K_s^0 candidates are reconstructed, the event is rejected. A K_s^0 candidate is defined as a system with a reconstructed $\pi^+\pi^-$ mass within a ± 30 MeV interval around the nominal K_s^0 mass. Only 1% of the original $K_s^0 K_s^0$ background remains after this cut.

In addition to the previous requirements, a cut $|\cos\theta^*| < 0.6$ is applied, where θ^* is the polar angle of the Λ in the two-photon centre-of-mass system, to match the experimental acceptance with the range of the theoretical predictions. Clean Λ and $\overline{\Lambda}$ signals are observed in the distributions of the $p\pi^-$ and $\overline{p}\pi^+$ masses, presented in Figures 2a and 2b. The Λ and $\overline{\Lambda}$ masses are found to be $m_\Lambda = 1.113 \pm 0.006$ GeV and $m_{\overline{\Lambda}} = 1.115 \pm 0.006$ GeV, respectively, in agreement with the nominal value of 1.116 GeV [15]. The final sample contains 66 inclusive $\Lambda\overline{\Lambda}$ candidates. They are selected within a radius of 40 MeV around the nominal Λ mass in the plane of the effective masses $m(p\pi^-)$ *vs.* $m(\overline{p}\pi^+)$, shown in Figures 2c and 2d. The remaining $K_s^0 K_s^0$ contamination is estimated by Monte Carlo simulation to be less than 1%. The normalisation of the $K_s^0 K_s^0$ Monte Carlo background is determined from our previous measurement of this channel [16]. Within the available statistics, the hypothesis of an isotropic distribution of the $\Lambda\overline{\Lambda}$ signal is verified.

2.2 Σ^0 identification

The reconstruction of Σ^0 and $\overline{\Sigma}^0$ candidates is performed by combining the selected Λ and $\overline{\Lambda}$ with photon candidates. A photon candidate is defined as a shower in the electromagnetic calorimeter with at least two adjacent crystals and an energy between 50 MeV and 200 MeV. Monte Carlo studies show that 91% of the photons emitted by a Σ^0 have an energy below 200

MeV, which is compatible with the nominal Σ^0 mass of 1.193 GeV. Photon isolation criteria are also applied; there must be no charged tracks within 200 mrad around the photon direction and the cosine of the angle between the antiproton and the photon directions must be less than 0.8. To identify the Σ^0, the mass difference $\Delta m = m(\mathrm{p}\pi\gamma) - m(\mathrm{p}\pi)$ is used, as presented in Figure 3. A Σ^0 candidate corresponds to the mass interval 47 MeV $< \Delta m <$ 107 MeV. Out of the 66 selected $\Lambda\overline{\Lambda}$ events, 31 have Σ^0 candidates.

3 Exclusive $\Lambda\overline{\Lambda}$ and $\Sigma^0\overline{\Sigma}^0$ identification

In order to select the events from the exclusive reactions $\gamma\gamma \to \Lambda\overline{\Lambda}$ and $\gamma\gamma \to \Sigma^0\overline{\Sigma}^0$, the transverse momentum of the four charged particles, P_T, is required to be less than 0.5 GeV. This cut rejects events containing contributions from other final states such as $\Xi^0\overline{\Xi}^0$ or $\Sigma^0(1385)\overline{\Sigma}^0(1385)$. Some of these states can still pass the P_T cut, but their contribution to the final sample is negligible, given the magnitude of their cross sections [6]. The P_T requirement rejects less than 8% of events corresponding to the exclusive final states $\Lambda\overline{\Lambda}$ and $\Sigma^0\overline{\Sigma}^0$. Since the photons emitted by the Σ^0 candidates have a low energy, they give a small contribution to the total transverse momentum imbalance. The final sample contains 33 events. The numbers of selected events for the different $\mathrm{e^+e^-}$ centre-of-mass energies are listed in Table 1. A typical $\Lambda\overline{\Lambda}$ event is shown in Figure 4.

The relative proportions of $\Lambda\overline{\Lambda}$ and $\Sigma^0\overline{\Sigma}^0$ final states in the sample are determined as follows. The event is labelled as $\Sigma^0\overline{\Sigma}^0$-like if a Σ^0 or a $\overline{\Sigma}^0$ candidate is observed and as $\Lambda\overline{\Lambda}$-like otherwise. With these criteria, 19 $\Lambda\overline{\Lambda}$-like and 14 $\Sigma^0\overline{\Sigma}^0$-like events are found in the data. The true fractions r_j $(j = \Lambda\overline{\Lambda}, \Sigma^0\overline{\Sigma}^0)$ of the two components are determined by a maximum extended likelihood fit with the constraint $r_{\Lambda\overline{\Lambda}} + r_{\Sigma^0\overline{\Sigma}^0} = 1$. The likelihood function to be maximized is:

$$\mathcal{L} = \frac{n_t^{N_t}\, e^{-n_t}}{N_t!} \prod_i \frac{n_i^{N_i}\, e^{-n_i}}{N_i!} \ ,$$

where N_t and n_t correspond respectively to the total number of observed and expected events, and N_i and n_i to the number of observed and expected i-like events. The latter is given by:

$$n_i = (\sum_j p_{ij} r_j) n_t \ ,$$

where p_{ij} is the probability of identifying an event corresponding to the final state j as i-like. The relative probabilities p_{ij} are determined by Monte Carlo and shown in Table 2 together with their statistical uncertainties. The fractions r_j and the number of events $n_t r_j$ obtained by the fit are given in Table 3.

The cross sections for the $\gamma\gamma \to \Lambda\overline{\Sigma}^0$ and $\gamma\gamma \to \Sigma^0\overline{\Lambda}$ processes are predicted to be negligible compared to the other channels [6]. In order to test this assumption, also an analysis with the three components $\Lambda\overline{\Lambda}$, $\Lambda\overline{\Sigma}^0 + \Sigma^0\overline{\Lambda}$ and $\Sigma^0\overline{\Sigma}^0$ is carried out. The $\Lambda\overline{\Sigma}^0 + \Sigma^0\overline{\Lambda}$ fraction is measured to be compatible with zero within a large uncertainty.

4 Results

The production cross sections $\sigma(\mathrm{e^+e^-} \to \mathrm{e^+e^-}\Lambda\overline{\Lambda})$ and $\sigma(\mathrm{e^+e^-} \to \mathrm{e^+e^-}\Sigma^0\overline{\Sigma}^0)$ are measured as a function of the centre-of-mass energy. They refer to the following phase-space cuts: the effective mass of the $\Lambda\overline{\Lambda}$ pair, $m_{\Lambda\overline{\Lambda}}$, less than 3.5 GeV, $|\cos\theta^*| < 0.6$ and $P_T < 0.5$ GeV. In

the cross section determination it is assumed that the fractions r_i are independent of $\sqrt{s}$. The results are summarised in Table 4.

The detection efficiency is determined by Monte Carlo for each data taking period. It takes into account the $\Lambda \to p\pi$ branching ratio and track geometrical acceptance ($\simeq 6\%$), the baryon identification criteria ($\simeq 26\%$) and the track trigger efficiency ($\simeq 10\%$). The efficiency of higher level triggers ($\simeq 90\%$) is estimated from the data themselves, using prescaled events. The contribution of the different selection cuts to the detection efficiency is detailed in Table 5. The total efficiencies for each data set are listed in Table 1.

The dominant source of systematic uncertainty is the selection procedure (7%); other sources are the finite Monte Carlo statistics (5%) and the determination of the trigger efficiency (3%). The Monte Carlo contribution includes the uncertainty on the p_{ij} probabilities used in the determination of the fractions r_i.

The cross sections $\sigma(\gamma\gamma \to \Lambda\overline{\Lambda})$ and $\sigma(\gamma\gamma \to \Sigma^0\overline{\Sigma}^0)$ in real photon collisions are extracted as a function of $W_{\gamma\gamma}$ by deconvoluting the two-photon luminosity function and the form factor [17]. They are presented in Table 6. For the $\gamma\gamma \to \Sigma^0\overline{\Sigma}^0$ case, the number of selected events as a function of $W_{\gamma\gamma}$ is obtained from the corresponding $m_{\Lambda\overline{\Lambda}}$ distribution, within a 4.0% uncertainty. The efficiencies and luminosity functions are evaluated for each $W_{\gamma\gamma}$ interval and centre-of-mass energy. The efficiencies increase with $W_{\gamma\gamma}$ reflecting the expected rise in the detector acceptance. The trigger and track identification efficiencies do not depend on $W_{\gamma\gamma}$. An additional systematic uncertainty of 5%, due to the choice of the photon form factor, is included.

Figure 5a compares the present $\sigma(\gamma\gamma \to \Lambda\overline{\Lambda})$ measurement with that of CLEO. The mass dependence of CLEO is steeper than the one we observe. Our data, fitted with a function of the form $\sigma \propto W^{-n}$, gives a value n = 7.6 ± 3.9. The quark-diquark model predicts n=6, and a three quark model n=10 [18]. In Figures 5b and 5c, the $\gamma\gamma \to \Lambda\overline{\Lambda}$ and $\gamma\gamma \to \Sigma^0\overline{\Sigma}^0$ cross section measurements are compared to the predictions of recent quark-diquark model calculations [6]. This model considers three different distribution amplitudes (DA) for the diquarks. The absolute predictions using the standard distribution amplitude (Standard DA) reproduce well our data. The asymptotic DA [19] and DZ-DA [20] models are excluded.

Acknowledgments

Author List

The L3 Collaboration:

P.Achard[20] O.Adriani[17] M.Aguilar-Benitez[24] J.Alcaraz[24,18] G.Alemanni[22] J.Allaby[18] A.Aloisio[28] M.G.Alviggi[28] H.Anderhub[46] V.P.Andreev[6,33] F.Anselmo[9] A.Arefiev[27] T.Azemoon[3] T.Aziz[10,18] P.Bagnaia[38] A.Bajo[24] G.Baksay[16] L.Baksay[25] S.V.Baldew[2] S.Banerjee[10] Sw.Banerjee[4] A.Barczyk[46,44] R.Barillère[18] P.Bartalini[22] M.Basile[9] N.Batalova[43] R.Battiston[32] A.Bay[22] F.Becattini[17] U.Becker[14] F.Behner[46] L.Bellucci[17] R.Berbeco[3] J.Berdugo[24] P.Berges[14] B.Bertucci[32] B.L.Betev[46] M.Biasini[32] M.Biglietti[28] A.Biland[46] J.J.Blaising[4] S.C.Blyth[34] G.J.Bobbink[2] A.Böhm[1] L.Boldizsar[13] B.Borgia[38] S.Bottai[17] D.Bourilkov[46] M.Bourquin[20] S.Braccini[20] J.G.Branson[40] F.Brochu[4] J.D.Burger[14] W.J.Burger[32] X.D.Cai[14] M.Capell[14] G.Cara Romeo[9] G.Carlino[28] A.Cartacci[17] J.Casaus[24] F.Cavallari[38] N.Cavallo[35] C.Cecchi[32] M.Cerrada[24] M.Chamizo[20] Y.H.Chang[48] M.Chemarin[23] A.Chen[48] G.Chen[7] G.M.Chen[7] H.F.Chen[21] H.S.Chen[7] G.Chiefari[28] L.Cifarelli[39] F.Cindolo[9] I.Clare[14] R.Clare[37] G.Coignet[4] N.Colino[24] S.Costantini[38] B.de la Cruz[24] S.Cucciarelli[32] J.A.van Dalen[30] R.de Asmundis[28] P.Déglon[20] J.Debreczeni[13] A.Degré[4] K.Deiters[44] D.della Volpe[28] E.Delmeire[20] P.Denes[36] F.DeNotaristefani[38] A.De Salvo[46] M.Diemoz[38] M.Dierckxsens[2] C.Dionisi[38] M.Dittmar[46,18] A.Doria[28] M.T.Dova[11,♯] D.Duchesneau[4] B.Echenard[20] A.Eline[18] H.El Mamouni[23] A.Engler[34] F.J.Eppling[14] A.Ewers[1] P.Extermann[20] M.A.Falagan[24] S.Falciano[38] A.Favara[31] J.Fay[23] O.Fedin[33] M.Felcini[46] T.Ferguson[34] H.Fesefeldt[1] E.Fiandrini[32] J.H.Field[20] F.Filthaut[30] P.H.Fisher[14] W.Fisher[36] I.Fisk[40] G.Forconi[14] K.Freudenreich[46] C.Furetta[26] Yu.Galaktionov[27,14] S.N.Ganguli[10] P.Garcia-Abia[5,18] M.Gataullin[31] S.Gentile[38] S.Giagu[38] Z.F.Gong[21] G.Grenier[23] O.Grimm[46] M.W.Gruenewald[1] M.Guida[39] R.van Gulik[2] V.K.Gupta[36] A.Gurtu[10] L.J.Gutay[43] D.Haas[5] R.Sh.Hakobyan[30] D.Hatzifotiadou[9] T.Hebbeker[1] A.Hervé[18] J.Hirschfelder[34] H.Hofer[46] M.Hohlmann[25] G.Holzner[46] S.R.Hou[48] Y.Hu[30] B.N.Jin[7] L.W.Jones[3] P.de Jong[2] I.Josa-Mutuberría[24] D.Käfer[1] M.Kaur[15] M.N.Kienzle-Focacci[20] J.K.Kim[42] J.Kirkby[18] W.Kittel[30] A.Klimentov[14,27] A.C.König[30] M.Kopal[43] V.Koutsenko[14,27] M.Kräber[46] R.W.Kraemer[34] W.Krenz[1] A.Krüger[45] A.Kunin[14] P.Ladron de Guevara[24] I.Laktineh[23] G.Landi[17] M.Lebeau[18] A.Lebedev[14] P.Lebrun[23] P.Lecomte[46] P.Lecoq[18] P.Le Coultre[46] J.M.Le Goff[18] R.Leiste[45] M.Levtchenko[26] P.Levtchenko[33] C.Li[21] S.Likhoded[45] C.H.Lin[48] W.T.Lin[48] F.L.Linde[2] L.Lista[28] Z.A.Liu[7] W.Lohmann[45] E.Longo[38] Y.S.Lu[7] K.Lübelsmeyer[1] C.Luci[38] L.Luminari[38] W.Lustermann[46] W.G.Ma[21] L.Malgeri[20] A.Malinin[27] C.Maña[24] D.Mangeol[30] J.Mans[36] J.P.Martin[23] F.Marzano[38] K.Mazumdar[10] R.R.McNeil[6] S.Mele[18,28] L.Merola[28] M.Meschini[17] W.J.Metzger[30] A.Mihul[12] H.Milcent[18] G.Mirabelli[38] J.Mnich[1] G.B.Mohanty[10] G.S.Muanza[23] A.J.M.Muijs[2] B.Musicar[40] M.Musy[38] S.Nagy[16] S.Natale[20] M.Napolitano[28] F.Nessi-Tedaldi[46] H.Newman[31] T.Niessen[1] A.Nisati[38] H.Nowak[45] R.Ofierzynski[46] G.Organtini[38] C.Palomares[18] D.Pandoulas[1] P.Paolucci[28] R.Paramatti[38] G.Passaleva[17] S.Patricelli[28] T.Paul[11] M.Pauluzzi[32] C.Paus[14] F.Pauss[46] M.Pedace[38] S.Pensotti[26] D.Perret-Gallix[4] B.Petersen[30] D.Piccolo[28] F.Pierella[9] M.Pioppi[32] P.A.Piroué[36] E.Pistolesi[26] V.Plyaskin[27] M.Pohl[20] V.Pojidaev[17] J.Pothier[18] D.O.Prokofiev[43] D.Prokofiev[33] J.Quartieri[39] G.Rahal-Callot[46] M.A.Rahaman[10] P.Raics[16] N.Raja[10] R.Ramelli[46] P.G.Rancoita[26] R.Ranieri[17] A.Raspereza[45] P.Razis[29] D.Ren[46] M.Rescigno[38] S.Reucroft[11] S.Riemann[45] K.Riles[3] B.P.Roe[3] L.Romero[24] A.Rosca[8] S.Rosier-Lees[4] S.Roth[1] C.Rosenbleck[1] B.Roux[30] J.A.Rubio[18] G.Ruggiero[17] H.Rykaczewski[46] A.Sakharov[46] S.Saremi[6] S.Sarkar[38] J.Salicio[18] E.Sanchez[24] M.P.Sanders[30] C.Schäfer[18] V.Schegelsky[33] S.Schmidt-Kaerst[1] D.Schmitz[1] H.Schopper[47] D.J.Schotanus[30] G.Schwering[1] C.Sciacca[28] L.Servoli[32] S.Shevchenko[31] N.Shivarov[41] V.Shoutko[14] E.Shumilov[27] A.Shvorob[31] T.Siedenburg[1] D.Son[42] P.Spillantini[17] M.Steuer[14] D.P.Stickland[36] B.Stoyanov[41] A.Straessner[18] K.Sudhakar[10] G.Sultanov[41] L.Z.Sun[21] S.Sushkov[8] H.Suter[46] J.D.Swain[11] Z.Szillasi[25,¶] X.W.Tang[7] P.Tarjan[16] L.Tauscher[5] L.Taylor[11] B.Tellili[23] D.Teyssier[23] C.Timmermans[30] Samuel C.C.Ting[14] S.M.Ting[14] S.C.Tonwar[10,18] J.Tóth[13] C.Tully[36] K.L.Tung[7] J.Ulbricht[46] E.Valente[38] R.T.Van de Walle[30] V.Veszpremi[25] G.Vesztergombi[13] I.Vetlitsky[27] D.Vicinanza[39] G.Viertel[46] S.Villa[37] M.Vivargent[4] S.Vlachos[5] I.Vodopianov[33] H.Vogel[34] H.Vogt[45] I.Vorobiev[34,27] A.A.Vorobyov[33] M.Wadhwa[5] W.Wallraff[1] X.L.Wang[21] Z.M.Wang[21] M.Weber[1] P.Wienemann[1] H.Wilkens[30] S.Wynhoff[36] L.Xia[31] Z.Z.Xu[21] J.Yamamoto[3] B.Z.Yang[21] C.G.Yang[7] H.J.Yang[3] M.Yang[7] S.C.Yeh[49] An.Zalite[33] Yu.Zalite[33] Z.P.Zhang[21] J.Zhao[21] G.Y.Zhu[7] R.Y.Zhu[31] H.L.Zhuang[7] A.Zichichi[9,18,19] G.Zilizi[25,¶] B.Zimmermann[46] M.Zöller[1]

1 I. Physikalisches Institut, RWTH, D-52056 Aachen, FRG[§]
 III. Physikalisches Institut, RWTH, D-52056 Aachen, FRG[§]
2 National Institute for High Energy Physics, NIKHEF, and University of Amsterdam, NL-1009 DB Amsterdam, The Netherlands
3 University of Michigan, Ann Arbor, MI 48109, USA
4 Laboratoire d'Annecy-le-Vieux de Physique des Particules, LAPP,IN2P3-CNRS, BP 110, F-74941 Annecy-le-Vieux CEDEX, France
5 Institute of Physics, University of Basel, CH-4056 Basel, Switzerland
6 Louisiana State University, Baton Rouge, LA 70803, USA
7 Institute of High Energy Physics, IHEP, 100039 Beijing, China[△]
8 Humboldt University, D-10099 Berlin, FRG[§]
9 University of Bologna and INFN-Sezione di Bologna, I-40126 Bologna, Italy
10 Tata Institute of Fundamental Research, Mumbai (Bombay) 400 005, India
11 Northeastern University, Boston, MA 02115, USA
12 Institute of Atomic Physics and University of Bucharest, R-76900 Bucharest, Romania
13 Central Research Institute for Physics of the Hungarian Academy of Sciences, H-1525 Budapest 114, Hungary[‡]
14 Massachusetts Institute of Technology, Cambridge, MA 02139, USA
15 Panjab University, Chandigarh 160 014, India.
16 KLTE-ATOMKI, H-4010 Debrecen, Hungary[¶]
17 INFN Sezione di Firenze and University of Florence, I-50125 Florence, Italy
18 European Laboratory for Particle Physics, CERN, CH-1211 Geneva 23, Switzerland
19 World Laboratory, FBLJA Project, CH-1211 Geneva 23, Switzerland
20 University of Geneva, CH-1211 Geneva 4, Switzerland
21 Chinese University of Science and Technology, USTC, Hefei, Anhui 230 029, China[△]
22 University of Lausanne, CH-1015 Lausanne, Switzerland
23 Institut de Physique Nucléaire de Lyon, IN2P3-CNRS,Université Claude Bernard, F-69622 Villeurbanne, France
24 Centro de Investigaciones Energéticas, Medioambientales y Tecnológicas, CIEMAT, E-28040 Madrid, Spain[♭]
25 Florida Institute of Technology, Melbourne, FL 32901, USA
26 INFN-Sezione di Milano, I-20133 Milan, Italy
27 Institute of Theoretical and Experimental Physics, ITEP, Moscow, Russia
28 INFN-Sezione di Napoli and University of Naples, I-80125 Naples, Italy
29 Department of Physics, University of Cyprus, Nicosia, Cyprus
30 University of Nijmegen and NIKHEF, NL-6525 ED Nijmegen, The Netherlands
31 California Institute of Technology, Pasadena, CA 91125, USA
32 INFN-Sezione di Perugia and Università Degli Studi di Perugia, I-06100 Perugia, Italy
33 Nuclear Physics Institute, St. Petersburg, Russia
34 Carnegie Mellon University, Pittsburgh, PA 15213, USA
35 INFN-Sezione di Napoli and University of Potenza, I-85100 Potenza, Italy
36 Princeton University, Princeton, NJ 08544, USA
37 University of Californa, Riverside, CA 92521, USA
38 INFN-Sezione di Roma and University of Rome, "La Sapienza", I-00185 Rome, Italy
39 University and INFN, Salerno, I-84100 Salerno, Italy
40 University of California, San Diego, CA 92093, USA
41 Bulgarian Academy of Sciences, Central Lab. of Mechatronics and Instrumentation, BU-1113 Sofia, Bulgaria
42 The Center for High Energy Physics, Kyungpook National University, 702-701 Taegu, Republic of Korea
43 Purdue University, West Lafayette, IN 47907, USA
44 Paul Scherrer Institut, PSI, CH-5232 Villigen, Switzerland
45 DESY, D-15738 Zeuthen, FRG
46 Eidgenössische Technische Hochschule, ETH Zürich, CH-8093 Zürich, Switzerland
47 University of Hamburg, D-22761 Hamburg, FRG
48 National Central University, Chung-Li, Taiwan, China
49 Department of Physics, National Tsing Hua University, Taiwan, China

References

[1] V. M. Budnev *et al.*, Phys. Rep. **15** (1974) 181.

[2] S. J. Brodsky et J. P. Lepage, Phys. Rev. **D 22** (1980) 2157.

[3] G. Farrar, E. Maina and F. Neri, Nucl. Phys. **B 259** (1985) 702; Nucl. Phys. **B 263** (1986) 746.

[4] CLEO collaboration, M. Artuso *et al.*, Phys. Rev. **D 50** (1994) 5484.

[5] M. Anselmino, F. Caruso, P. Kroll and W. Schweiger, Int. Mod. Phys. **A 4** (1989) 5213.

[6] C. F. Berger, B. Lechner and W. Schweiger, Fizika **B 8** (1999) 371;
C. F. Berger, *Exclusive Two-Photon Reactions in the Few-GeV Region*, Diploma Thesis, Graz University, 1997;
C. F. Berger and W. Schweiger, private communication.

[7] L3 Collab., B. Adeva *et al.*, Nucl. Instr. Meth. **A 289** (1990) 35;
L3 Collab., O. Adriani *et al.*, Phys. Rep. **236** (1993) 1;
M. Chemarin *et al.*, Nucl. Instr. Meth. **A 349** (1994) 345;
M. Acciarri *et al.*, Nucl. Instr. Meth. **A 351** (1994) 300;
I. C. Brock *et al.*, Nucl. Instr. Meth. **A 381** (1996) 236;
A. Adam *et al.*, Nucl. Instr. Meth. **A 383** (1996) 342.

[8] P. Béné *et al.*, Nucl. Inst. Meth. **A 306** (1991) 150;
D. Haas *et al.*, Nucl. Inst. Meth. **A 420** (1991) 101.

[9] F. L. Linde, *Charm Production in Two-Photon Collisions*, Ph.D. Thesis, Rijksuniversiteit Leiden, 1988.

[10] R. Brun *et al.*, GEANT 3.15 preprint CERN DD/EE/84-1 (Revised 1987).

[11] H. Fesefeldt, RWTH Aachen report PITHA 85/2, 1985.

[12] CLEO collaboration, S. Anderson *et al.*, Phys. Rev. **D 56** (1997) 2485.

[13] TPC/2γ collaboration, H. Aihara *et al.*, Phys. Rev. **D 40** (1989) 2772.

[14] VENUS collaboration, S. Uehara *et al.*, Z.Phys. **C 69** (1996) 597.

[15] Particle Data Group, D. E. Groom *et al.*, Eur. Phys. J. **C 15** (2000) 1.

[16] L3 collaboration, M. Acciarri *et al.*, Phys. Lett. **B 501** (2001) 173.

[17] G. A. Schuler, hep-ph/9610406, CERN-TH/96-297.

[18] S. J. Brodsky and G. R. Farrar, Phys. Rev. Lett. **31** (1973) 1153.

[19] P. Kroll, M. Schürmann and W. Schweiger, Z. Phys. **A 338** (1991) 339.

[20] Z. Dziembowski, Phys. Rev. **D 37** (1988) 2030.

$\sqrt{s}$ (GeV)	Luminosity (pb^{-1})	Efficiency (%)	Events
91	157	2.38 ± 0.11	8
$161-172$	20	1.72 ± 0.07	3
183	52	1.97 ± 0.09	1
189	172	1.78 ± 0.07	3
$192-202$	230	1.94 ± 0.07	10
$205-208$	213	1.75 ± 0.07	8

Table 1: Integrated luminosity, overall efficiency and number of selected $e^+e^- \rightarrow e^+e^-\Lambda\overline{\Lambda}$ and $e^+e^- \rightarrow e^+e^-\Sigma^0\overline{\Sigma}^0$ events for each data taking period. The efficiency refers to the phase-space cuts: $2.23 < m_{\Lambda\overline{\Lambda}} < 3.5$ GeV, $|\cos\theta^*| < 0.6$ and $P_T < 0.5$ GeV. The quoted uncertainties are statistical.

Identified as	N_i	Selection probability p_{ij} (%)	
		Generated as $\Lambda\overline{\Lambda}$	Generated as $\Sigma^0\overline{\Sigma}^0$
$\Lambda\overline{\Lambda}$-like	19	88.0 ± 0.8	39.1 ± 1.0
$\Sigma^0\overline{\Sigma}^0$-like	14	12.0 ± 0.8	60.9 ± 1.0

Table 2: Numbers of observed events N_i identified as $\Lambda\overline{\Lambda}$-like and $\Sigma^0\overline{\Sigma}^0$-like and relative probabilities p_{ij} of identifying an event generated in the final state j as i-like.

Final state	Fraction r_j	Events $n_t r_j$
$\Lambda\overline{\Lambda}$	0.38 ± 0.18	12.5 ± 6.1
$\Sigma^0\overline{\Sigma}^0$	0.62 ± 0.18	20.5 ± 6.5

Table 3: Results of the fit for the fractions r_j and the number $n_t r_j$ of $\Lambda\overline{\Lambda}$ and $\Sigma^0\overline{\Sigma}^0$ final states.

$\sqrt{s}$ (GeV)	$\sigma(e^+e^- \rightarrow e^+e^-\Lambda\overline{\Lambda})$ (pb)	$\sigma(e^+e^- \rightarrow e^+e^-\Sigma^0\overline{\Sigma}^0)$ (pb)
91	$0.81 \pm 0.48 \pm 0.07$	$1.33 \pm 0.61 \pm 0.12$
$161-208$	$0.75 \pm 0.39 \pm 0.07$	$1.23 \pm 0.43 \pm 0.11$

Table 4: The $e^+e^- \rightarrow e^+e^-\Lambda\overline{\Lambda}$ and $e^+e^- \rightarrow e^+e^-\Sigma^0\overline{\Sigma}^0$ cross sections for $2.23 < m_{\Lambda\overline{\Lambda}} < 3.5$ GeV, $|\cos\theta^*| < 0.6$ and $P_T < 0.5$ GeV. The first uncertainty is statistical, the second systematic.

Cut	Acceptance (%)
Four tracks	10
Two secondary vertices	55
Photon conversion rejection	93
dE/dx compatibility	98
dE/dx or E_T/p_T	77
$K_s^0 K_s^0$ rejection	92
$|\cos\theta^*|$	83
Λ vs $\overline{\Lambda}$ mass	94
P_T	92
Total	2.5

Table 5: Average acceptance of the different selection cuts used in the analysis. The overall efficiency takes also into account the acceptance of the trigger system ($\simeq 80\%$).

$W_{\gamma\gamma}$ (GeV)	$\langle W_{\gamma\gamma}\rangle$ (GeV)	$\sigma(\gamma\gamma \to \Lambda\overline{\Lambda})$ (pb)	$W_{\gamma\gamma}$ (GeV)	$\langle W_{\gamma\gamma}\rangle$ (GeV)	$\sigma(\gamma\gamma \to \Sigma^0\overline{\Sigma}^0)$(pb)
$2.2 - 2.5$	2.34	$226 \pm 111 \pm\ \ 23$	$2.4 - 2.7$	2.51	$369 \pm 116 \pm\ \ 41$
$2.5 - 2.7$	2.59	$92 \pm\ \ 45 \pm\ \ 10$	$2.7 - 2.9$	2.77	$151 \pm\ \ 48 \pm\ \ 17$
$2.7 - 3.1$	2.86	$44 \pm\ \ 22 \pm\ \ \ \ 5$	$2.9 - 3.3$	3.06	$72 \pm\ \ 23 \pm\ \ \ \ 8$
$3.1 - 3.5$	3.27	$18 \pm\ \ \ \ 9 \pm\ \ \ \ 2$	$3.3 - 3.8$	3.50	$30 \pm\ \ \ \ 9 \pm\ \ \ \ 3$

Table 6: The $\gamma\gamma \to \Lambda\overline{\Lambda}$ and $\gamma\gamma \to \Sigma^0\overline{\Sigma}^0$ cross sections as a function of $W_{\gamma\gamma}$ for $|\cos\theta^*| < 0.6$ and $P_T < 0.5$ GeV. The central value $\langle W_{\gamma\gamma}\rangle$ of each bin corresponds to an average according to a W^{-8} distribution. The first uncertainty is statistical, the second systematic.
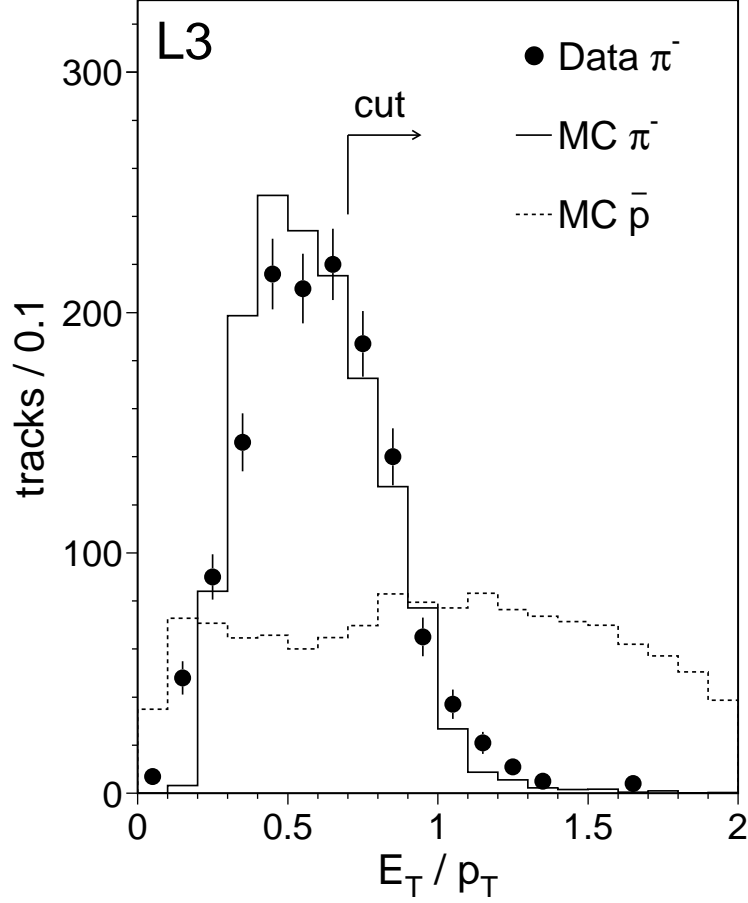
Figure 1: Distribution of the ratio of the transverse energy deposited in the electromagnetic calorimeter, E_T, and the transverse momentum, p_T, for pions and antiprotons. The π^- data distribution is obtained from a high purity $K_s^0 K_s^0$ sample [16]. The π^- Monte Carlo distribution corresponds to a simulated $e^+e^- \to e^+e^- K_s^0 K_s^0$ sample normalized to the number of $K_s^0 K_s^0$ observed in data [16]. The antiproton distribution is obtained from simulated $e^+e^- \to e^+e^- \Lambda \overline{\Lambda}$ events, with arbitrary normalization.
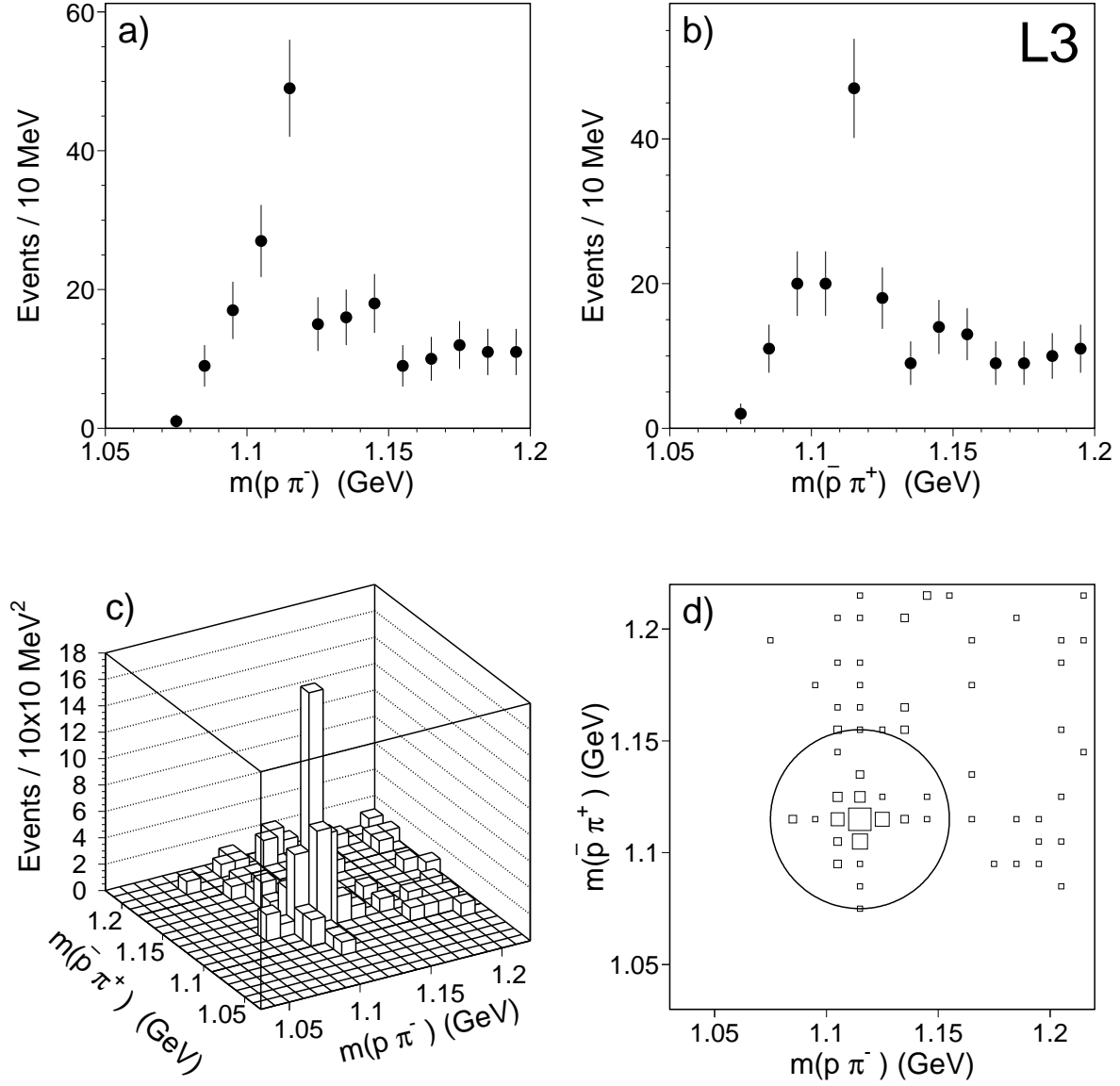
Figure 2: Effective mass distribution of the a) $p\pi^-$ system and b) $\overline{p}\pi^+$ system. The two dimensional distribution is shown in c) and d). A radius of 40 MeV around the nominal mass value of m_Λ defines the inclusive $\Lambda\overline{\Lambda}$ sample.
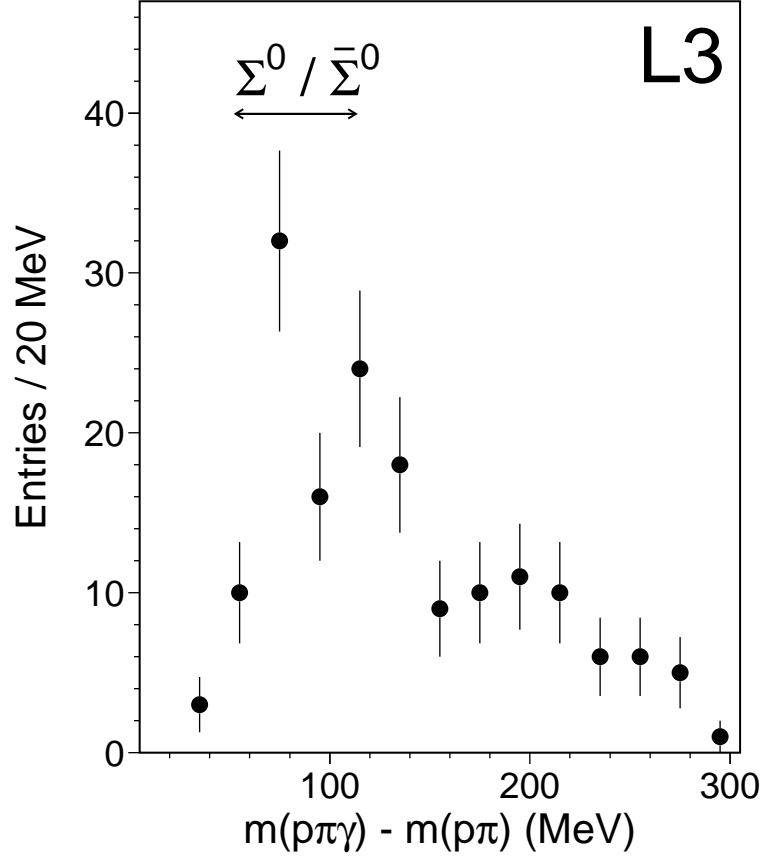
Figure 3: Distribution of the mass difference between the $\Lambda\gamma$ ($p\pi\gamma$) and the Λ ($p\pi$) systems. All possible combinations of a photon and a Λ or $\overline{\Lambda}$ candidate are shown.
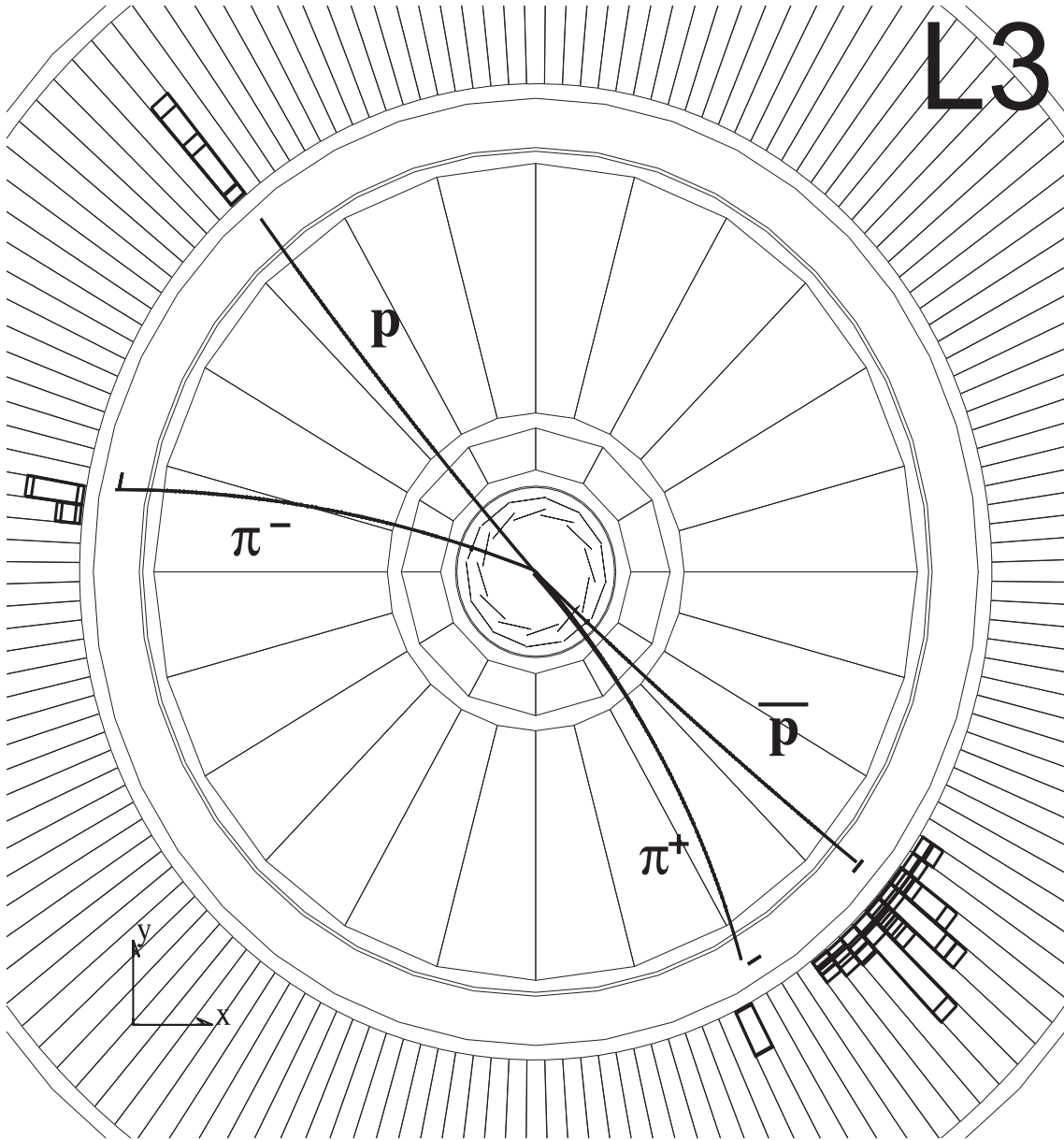
Figure 4: A typical $\gamma\gamma \to \Lambda\overline{\Lambda}$ event, displayed in the transverse plane. It illustrates the higher momentum of the proton and antiproton in the Λ and $\overline{\Lambda}$ decays and the separation in the electromagnetic calorimeter between the large antiproton signal and the small energy deposit of pions and protons.
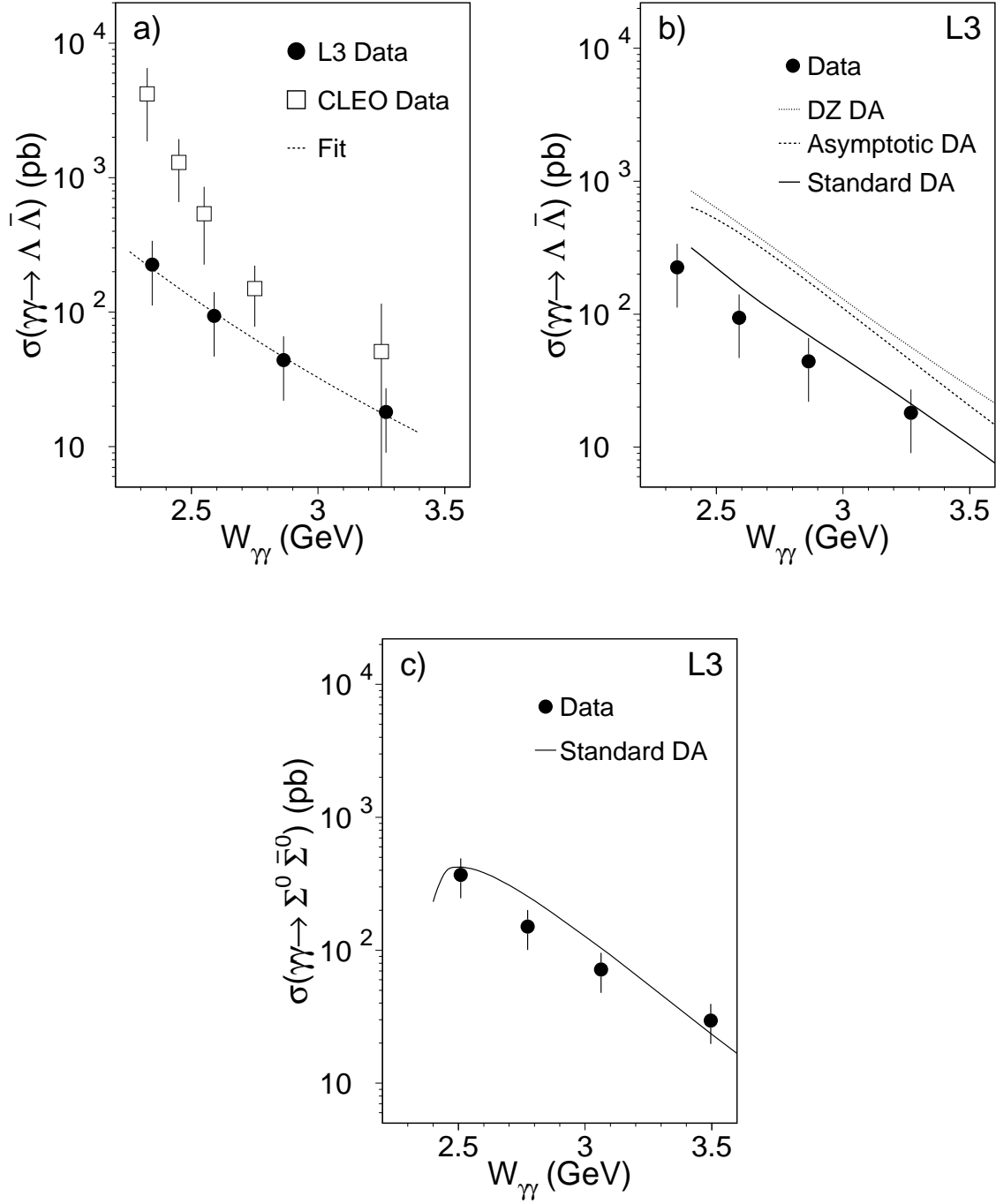
Figure 5: Measurements of the $\gamma\gamma \to \Lambda\overline{\Lambda}$ and $\gamma\gamma \to \Sigma^0\overline{\Sigma}^0$ cross sections as a function of $W_{\gamma\gamma}$. In a) the $\gamma\gamma \to \Lambda\overline{\Lambda}$ cross section is compared to the one obtained by CLEO [4]. The dashed line shows the power law fit described in the text. In b) and c) the $\sigma(\gamma\gamma \to \Lambda\overline{\Lambda})$ and $\sigma(\gamma\gamma \to \Sigma^0\overline{\Sigma}^0)$ measurements are compared to the calculations of Reference 6. Statistical and systematic uncertainties are added in quadrature.

15